Talanta 210 (2020) 120647

Contents lists available at ScienceDirect

Talanta

journal homepage: www.elsevier.com/locate/talanta

Development of an enzymatic biosensor to determine eugenol in dental samples

Jimena Claudia Lopez, María Alicia Zon**, Héctor Fernández, Adrian Marcelo Granero*

Departamento de Química, Grupo GEANA, Instituto para el Desarrollo Agroindustrial y de la Salud (IDAS), Facultad de Ciencias Exactas, Físico-Químicas y Naturales, Universidad Nacional de Río Cuarto, Agencia Postal Nº 3, 5800, Río Cuarto, Argentina

ARTICLE INFO

Keywords:
Enzymatic biosensor
Soybean peroxidase enzyme
Chemically reduced graphene oxide
β-Cyclodextrin's
Eugenol

ABSTRACT

A GCE/CRGO-βCD's/ADA-SPE/AuNPs biosensor was successfully developed to determine eugenol in dental samples. The optimal conditions to construct the biosensor were obtained from an experimental design based on the response surfaces methodology. The GCE/CRGO-βCD/ADA-SPE/AuNPs biosensor exhibited a very good analytical performance for the quantification of eugenol. Thus, it shows a linear range between 1.3×10^{-8} and 1×10^{-5} mol L^{-1}, with a sensitivity of (5.3 ± 0.3) x 10^{-3} A mol^{-1} L. The limits of detection and quantification were 4×10^{-9} mol L^{-1} and 1.3×10^{-8} mol L^{-1}, respectively. Biosensors had an intraday and inter day reproducibility of 5% and 8%, respectively. The repeatability was of 3%, and the stability was 21 days (a decrease of 30% in current responses was observed after the fourth week). Recovery studies were performed in order to validate the proposed method. Recovery percentages were between 94 and 108%. A value of the apparent Michaellis-Menten constant, K_M^{app}, of 3.1×10^{-6} mol L^{-1} was obtained using both Lineweaver-Burk and Eadi-Hofstee methods.

1. Introduction

A semi-volatile compound, eugenol or 4-allyl-2-methoxyphenol (EUG, Fig. 1) is a lipophilic antioxidant. It is a liquid at room temperature, pale yellow and of oily consistency. It is found mainly in clove oil [1], and can be extracted from cloves, cinnamon and other aromatic compounds [2–5].

EUG is a compound with remarkably unique medicinal properties and biological activities such as antimicrobial, anti-inflammatory, antifungal, antiviral, analgesic, antimutagenic, antiseptic, antioxidant and anti-cancer [6–8]. Due to the various properties of EUG, it has a wide application in the pharmaceutical, agricultural, fragrance, flavor, cosmetic, food and various other industries as well as in dentistry and medicine [9,10].

EUG is natural plant-based product. According to the World Health Organization, the maximum daily human intake recommended is 2.5 mg kg^{-1} body weight [11]. Exceeding this limit may cause serious and fatal problems such as arrhythmia, digestive problems, and an increase in blood pressure, vomiting and liver failure. Thus, the amount of EUG in the pharmaceutical and food industries must be strictly controlled to prevent harm to human health [12]. Therefore, a quantitative analysis of EUG is of great interest.

Quantitative methods have been reported extensively for the compositional analysis of plant extracts [13], dental materials [14], cosmetics [15] and flavor additive [16]. The usually proposed methods for the determination of EUG are based on gas chromatography (GC) [17,18] and high performance liquid chromatography (HPLC) [19].

Another interesting alternative to determine EUG is the use of electroanalytical methods. Compared to the conventional methods such as HPLC, GC and mass spectrometry, electrochemical methods have certain advantages for detecting several analytes, owing to their rapid analysis, low cost, high sensitivity and simplicity. Therefore, EUG was determined at carbon paste electrodes (CPE) chemically modified with gold metallic nanoparticles (AuNPs) by differential pulse voltammetry (DPV) in pH 8 phosphate buffer solutions (PBS) using both the commercial reagent, and different real samples. A great catalytic effect and a marked increase in peak currents were observed when the EUG electro-oxidation was studied at these modified electrodes (AuNPs/CPE) compare to the bare CPE [20]. On the other hand, the EUG electrochemical oxidation mechanism was studied at glassy carbon electrodes (GCE) modified with Cu doped AuNPs (Cu@AuNPs/GCE) using the Britton Robinson buffer as the supporting electrolyte in the

* Corresponding author.
** Corresponding author.
E-mail addresses: jlopez@exa.unrc.edu.ar (J.C. Lopez), azon@exa.unrc.edu.ar (M.A. Zon), hfernandez@exa.unrc.edu.ar (H. Fernández), agranero@exa.unrc.edu.ar (A.M. Granero).

https://doi.org/10.1016/j.talanta.2019.120647
Received 8 October 2019; Received in revised form 12 December 2019; Accepted 13 December 2019
Available online 16 December 2019
0039-9140/ © 2019 Published by Elsevier B.V.

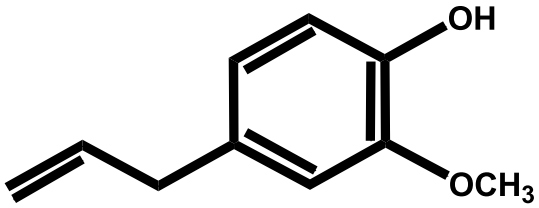

Fig. 1. Chemical structure of eugenol.

pH range from 2 to 7.80. These authors found that the current of the EUG main oxidation peak was higher at pH 2 than at other pH. In addition, the oxidation peak was shifted at less positive potentials as the pH increased. They also observed that at pH 2 the EUG oxidation peak was much better defined at the modified electrode than at the bare GCE. This modified electrode was then used to determine EUG in spice and curry powder samples [21]. Besides, the EUG electro-oxidation mechanism was also studied at carbon paste electrodes modified with graphene (G-CPE) in Britton Robinson buffer at pH 2. These studies were carried out by using density functional theory computations and mass spectroscopy analysis. In addition, DPV was used to generate the calibration curve, which allowed determining EUG in a pharmaceutical formulation [22]. Moreover, a GCE modified with a graphene-carbon nanotubes-ionic liquid composite (G-CNTs-IL) was used to fabricate an electrochemical sensor to determine EUG based on a molecularly imprinted polymer (MIP), which was generated using p-amino thiophenol and p-amino benzoic acids as monomers and EUG as the template. This electrochemical sensor was used to determine EUG in real samples such as curry powder, perfume and capsules by using linear sweep voltammetry [23].

On the other hand, biosensors have been proposed as an efficient analytical tool for the determination of phenolic and polyphenolic compounds, exhibiting advantages such as the minimal preparation of the sample, selectivity, sensitivity, reproducibility, rapid response time and simple use for continuous on-site analysis [24].

The soybean peroxidase enzyme (SPE) is a good biological element in the development of biosensors due to some intrinsic characteristics, i.e., it has higher thermal stability and it can maintain its bioactivity in a wider pH range than other peroxidases [25,26]. This enzyme has successfully been used by us for the development of biosensors to determine hydrogen peroxide and the sterigmatocystin mycotoxin [27,28].

On the other hand, the most of the graphene (G) used in the development of electrochemical biosensors is reduced graphene oxide (RGO) [29]. Generally, the graphene oxide (GO) can form a stable dispersion in water, due to the high content of oxygenated groups. Chemically reduced graphene oxide (CRGO) is obtained if these functional groups are removed through chemical reduction. Thus, the CRGO loses its dispersibility in water and can be precipitated due to high interlayer interactions. An improvement in water dispersibility is achieved by the modification of the graphene sheets introducing new functional molecules between layers. In this way, β-cyclodextrin's (βCD's) can be used to modify the CRGO layers in order to significantly increase its water solubility [30]. βCD's can attach themselves to CRGO layers through strong hydrogen bonds, resulting in a more hydrophilic CRGO. Thus, the CRGO functionalized with βCD's has the properties of large surface area, high conductivity, and supra-molecular recognition and enrichment capacity of the βCD's to be used as an electrochemical sensor [31]. βCD's have also been used to immobilize enzymes modified with adamantane or 1- adamantane carboxylic acid (ADA), through host-guest interactions. Thus, this interesting proposal has been used in different occasions to modify enzymes with ADA to generate enzymatic biosensors [32–34].

In addition, the use of AuNPs can improve some characteristics of biosensors due to their excellent properties such as a high catalytic activity, small size, large surface area, effective mass transport. In addition, they are friendly with the environment. AuNPs modified electrodes can reduce over-potentials and to improve electrocatalysis. Particularly, modified electrodes with G or G derivatives and AuNPs have been developed in order to improve their performance as sensors. A sinergistic effect has been observed which increases the analytical signal due to the presence of two types of nano-structured materials [35–37].

In this paper, we propose the development of an amperometric biosensor based on SPE to determine EUG in dental samples. The biosensor is based on the immobilization of a conjugate obtained by ADA and SPE (ADA-SPE) at a GCE modified with a composite of CRGO and βCD's (βCD's-CRGO). The use of nano-material CRGO is necessary to immobilize βCD's on the electrode surface. AuNPs were also electrodeposited at the modified electrode. Our enzymatic biosensor showed a very good analytical performance for the quantification of EUG in dental samples.

2. Materials and methods

2.1. Reagents

EUG, ADA, βCD's, tetrachloroauric acid (III) trihydrate and N-(3-dimethylaminopropyl)-N′-ethylcarbodiimide hydrochloride (EDAC) were purchased from Sigma–Aldrich. Ethanol, KH_2PO_4, K_2HPO_4, HCl and NaOH were Merck p.a. Ultrapure water (ρ = 18 MΩ cm) was obtained from a Millipore-Milli Q system. Stock solutions of EUG were 0.64 mol L^{-1} in ethanol. They were protected from light, and kept in the refrigerator. The corresponding working solutions were prepared daily by adding different aliquots of the stock solution in the corresponding reaction media.

PBS of different pH were prepared using 0.2 mol L^{-1} K_2PO_4H/KPO_4H_2, adjusting the pH by adding different volumes of 1 mol L^{-1} HCl or 1 mol L^{-1} NaOH solutions as corresponding.

H_2O_2 (Merck p.a.) solutions were prepared daily. Their concentrations were determined from uv–vis absorption spectrophotometric measurements at λ = 240 nm [38].

SPE was kindly provided by Dr G. J. Levin from Centro de Investigaciones y Transferencia de Entre Ríos, Gualeguachú, Entre Ríos, Argentina. SPE was purified from soybean hulls as a single isoenzyme using a procedure described in literature [27]. The enzyme concentration was determined from uv–vis absorption spectrophotometric measurements at λ = 403 nm [39].

2.2. Apparatus

Amperometric and cyclic voltammetry (CV) measurements were performed using a BAS Epsilon potentiostat, with electrochemical software incorporated. The scan rate (v) was 0.100 V s^{-1}. Electrochemical impedance spectroscopy (EIS) experiments were carried out with an AutoLab PGSTAT 30 potentiostat with FRA 4.9 software incorporated. These measurements were performed in 1×10^{-3} mol L^{-1} of $K_4[Fe(CN)_6]$ and $K_3[Fe(CN)_6]$ + 0.1 mol L^{-1} KCl aqueous solution at an equilibrium potential of 0.234 V vs. Ag/AgCl. A sine wave perturbation of 5 mV was applied to electrodes. The ac frequency was varied from 0.5 Hz to 10 kHz. The Nyquist plots were fitted by the FRA impedance software using the equivalent circuits described in Section 3.3.1. A conventional three electrode cell was used in all electrochemical measurements. The working electrode was a glassy carbon (GCE) disk (BAS, φ = 3 mm). The reference and counter electrodes were Ag/AgCl (3 mol L^{-1} NaCl) and a large area Pt sheet, respectively. The volume of the electrochemical cell was 2 mL. The solutions were deoxygenated by bubbling N_2 for 15 min prior to the experiments.

An uv–vis spectrophotometer Hewlett Packard, model HP8453 was used for spectrophotometric measurements. The cells had an optical path of 1 cm.

SEM measurements (Carl Zeiss Sigma with Zeiss-MMSTEM detector and EDS micro-analyzer, Oxford-AZtec x MAx 80) were used to characterize the different stages during the modification of the electrode surface.

2.3. Synthesis of the ADA-SPE conjugate

The ADA-SPE conjugate was carried out following a method proposed by Lv et al. [29].

Thus, a reaction mixture composed of 750 μL of the SPE 1.55×10^{-4} mol L^{-1} (31 μmol L^{-1}), 27 mg of ADA (0.031 mol L^{-1}) and 50 mg of EDAC (0.05 mol L^{-1}) in 5 mL of a solution 0.2 mol L^{-1} pH 6.0 PBS was stirred overnight in the refrigerator at 4 °C. Then, the reaction mixture was dialyzed in 0.2 mol L^{-1} pH 6.0 PBS during three days in a refrigerator. The conjugate was kept in the freezer while it was not used.

2.4. Synthesis of the CRGO-βCD's composite

GO was synthesized following the methodology proposed by Marcano et al. [40].

The CRGO-βCD's composite was synthesized following a procedure similar to one described in literature [41]. Thus, 5 mL of a GO dispersion (0.5 mg mL^{-1}) were mixed in a glass bottle with 5 mL of an aqueous solution of βCD's (80 mg mL^{-1}) and 0.375 mL of ammonia solution (28% w/w). Then, 0.01 mL of hydrazine solution (50% w/w) were added and stirred during 5 min. Then, the mixture was transferred to a water bath at 60 °C during 3.5 h. Once at room temperature, the dispersion was centrifuged at 10000 rpm during 5 min and washed several times with distilled water to remove the excesses of hydrazine and βCD's.

2.5. Synthesis of the gold nanoparticles

The synthesis of AuNPs was carried out by electro-deposition. Thus, the GCE/CRGO-βCD's/ADA-SPE was added to a solution 5×10^{-4} mol L^{-1} $HAuCl_4$ in pH 7.0 PBS and a potential was applied during a certain time. The variation in the biosensor response was studied from an experimental design, to choose the best applied potential (E_{app}) and the electro-deposition time (t_{app}).

2.6. Preparation of electrodes

Pretreatment of GCE: the electrodes were polished with alumina slurries of 0.30 and 0.05 μm for 1 min each, and sonicated in water during 30 s.

Preparation of GCE/CRGO-βCD's: the polished GCE was modified with CRGO-βCD's composite (GCE/CRGO-βCD's) by dropping an aliquot of 10 μL of the composite on the top of the electrode and allowing drying during 30 min at 37 °C.

Preparation of GCE/CRGO-βCD's/ADA-SPE: the GC/CRGO-βCD's/ADA-SPE was generated by immersion of GCE/CRGO-βCD's in a solution ADA-SPE during 4 h in pH 7.0 PBS. Then, the GCE/CRGO-βCD's/ADA-SPE was washed with pH 7.00 PBS to remove remnants of the ADA-SPE conjugate, no bonded to the GCE/CRGO-βCD's.

Preparation of GCE/CRGO-βCD's/ADA-SPE/AuNPs: the AuNPs were electro-deposited by applying a potential of −0.25 V (vs. Ag/AgCl, 3 mol L^{-1} NaCl) at GCE/CRGO-βCD's/ADA-SPE during 20 s in 0.5 mmol L^{-1} $HAuCl_4$ + pH 7.0 PBS.

2.7. Experimental design

The construction of the enzymatic amperometric biosensor to determine EUG depends on several variables that affect its analytical performance. Thus, the factors involved in the construction of the biosensor were first identified. They were:

- Volume of the CRGO-βCD's composite deposited at the GCE surface.
- Incubation time of GCE/CRGO-βCD's in the ADA-SPE solution.
- Generation stage of AuNPs (before or after of GCE/CRGO-βCD's incubation in the ADA-SPE solution).
- Electro-deposition potential of AuNPs.
- Electro-deposition time of AuNPs.
- Stabilization time of the biosensor in PBS (baseline stabilization).
- Potential applied to GCE/CRGO-βCD's/ADA-SPE/AuNPs during the stabilization process and EUG aggregates.
- pH: the pH value at which the amperometric measurements were carried out.
- H_2O_2 concentration ($c^*_{H_2O_2}$) at which the amperometric measurements were performed.

Then, the factors that were significant to obtain the maximum sensitivity were selected. Thus, a fractional factorial design (FFD), 2^{9-4}, was used to study the nine factors mentioned above [42]. Table S1 (Supplementary material) shows the levels chosen for each factor.

Finally, the optimization stage of the significant factors was carried out in order to optimize biosensor responses. Therefore, a composite central design (CCD) with five factors at five levels was used. The response to optimize was the slope of the EUG calibration curve. From these results, 29 experiments were performed. The levels of significant factors are shown in Table S2 (Supplementary material) for EUG concentrations in the range from 1×10^{-7} to 1×10^{-4} mol L^{-1}.

3. Results and discussion

3.1. Characterization of the ADA-SPE conjugate

To verify the enzymatic activity of SPE after conjugation with ADA, its enzymatic kinetics was studied using H_2O_2 as substrate and EUG as co-substrate.

Thus, Fig. S1 (Supplementary material) shows uv–vis absorption spectrum of EUG (line 1, Fig. S1) and uv–vis absorption spectra recorded during the development of the enzymatic reaction using the ADA-SPE conjugate (lines 2 to 17, Fig. S1). From these results, it can be deduced that the enzyme maintains its catalytic activity in the ADA-SPE conjugate, since it is possible to observe the appearance of an absorption band at λ = 358 nm, which corresponds to an unstable intermediary of the enzymatic reaction as it was previously discussed [43].

Through the use of MCR-ALS algorithm, the concentration profiles of the different species involved in the enzymatic kinetics were determined. Thus, Fig. S2 (Supplementary material) shows the responses of c^*_{EUG} vs. time obtained using SPE as well as ADA-SPE conjugate.

As it can be observed, the decay in the EUG concentration is lower with the ADA-SPE conjugate than with SPE at short times. However, both decays are practically the same after 140 s.

3.2. Characterization of the synthesis of CRGO-βCD's composite

The characterization of CRGO-βCD's composite was carried out through uv–vis absorption spectroscopy measurements. Thus, GO shows a maximum absorption at λ = 230 nm, assigned to a transition π → π* of the aromatic double bonds and a shoulder at λ = 300 nm, assigned to a transition n → π* of C═O bond (Fig. S3 in Supplementary material).

When the reduction of the GO occurs in the presence of βCD's to obtain CRGO-βCD's (see section 2.4.) the uv–vis spectrum changes its shape. Thus, the absorption band due to the n→π* transition is markedly diminished due to the reduction of the C═O groups of the GO (Fig. S3 in Supplementary material).

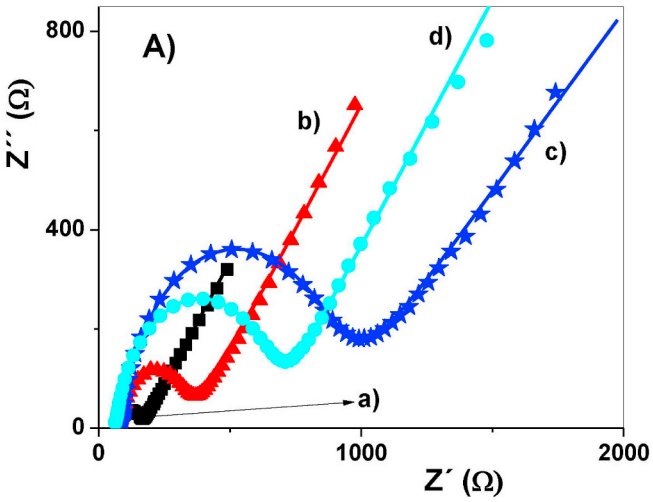

Fig. 2. A) Nyquist plots for a) GCE, b) GCE/CRGO-βCD's, c) GCE/CRGO-βCD's/ADA-SPE and d) GCE/CRGO-βCD's/ADA-SPE/AuNPs. The solid lines correspond to the fitted impedance spectra with the corresponding equivalent circuits. B) Equivalent circuits that best fitted the experimental data for the different electrodes a) Randless equivalent circuit and b) equivalent circuit proposed by Casero et al. [44].

3.3. Characterization of the different stages of assembly of the biosensor

3.3.1. Electrochemical impedance spectroscopy and cyclic voltammetry

The different stages of assembly of the biosensor were characterized by EIS and CV. Fig. 2A shows the Nyquist plots for a) GCE, b) GCE/CRGO-βCD's, c) GCE/CRGO-βCD's/ADA-SPE and d) GCE/CRGO-βCD's/ADA-SPE/AuNPs. Fig. 2B shows the equivalent circuits that best fitted the experimental data for the different electrodes (see below). They were the Randless equivalent circuit (a) and the equivalent circuit proposed by Casero et al. (b) [44].

Nyquist plots show two well differentiated sections. On the one hand, semicircles can be observed at high frequencies which are related to the kinetic control of electron transfer of the redox couple. On the other hand, a linear portion is also observed at low frequency, which is related to the diffusion control of the redox couple.

Thus, the Nyquist plot shows for the bare GCE a semicircle at high frecuencies, and a straigh line at low frecuencies. The best fitting was obtained when the Randles equivalent circuit was used (Fig. 2B a). In this circuit, R_S is the resistance of the solution, CPE_{dl} is the constant phase element of the electrical double layer, R_{ET} is the electron transfer resistance and W is the Warburg element. From the best fitting, a value of R_{ET} = 84 Ω was obtained.

In the case of the modified electrodes (GCE/CRGO-βCD's, GCE/CRGO-βCD's/ADA-SPE and GCE/CRGO-βCD's/ADA-SPE/AuNPs), the equivalent circuit that best fitted the experimental data was the equivalent circuit shown in Fig. 2B b. The CPE_c in this equivalent circuit is a constant phase element, which refers to the presence of different nano-structures at the modified GCE. These nano-structures acts as a dielectric that difficult the electron transfer of $[Fe(CN)_6]^{-4/-3}$ redox couple.

The CPE_c for the GCE/CRGO-βCD's represents the oxygenated functional groups that were not affected by the reduction of the GO by hydrazine. From the fitting, the following value was obtained: R_{ET} = 273 Ω.

The R_{ET} value increased for GCE/CRGO-βCD's/ADA-SPE (compared with GCE/CRGO-βCD's) due to the incorporation of the ADA-SPE composite which acts as a dielectric layer, hindering the electron transfer of $[Fe(CN)_6]^{-4/-3}$ redox couple. From the best fitting, a value of R_{ET} = 806 Ω was obtained for this modified electrode.

The incorporation of the AuNPs at GCE/CRGO-βCD's/ADA-SPE

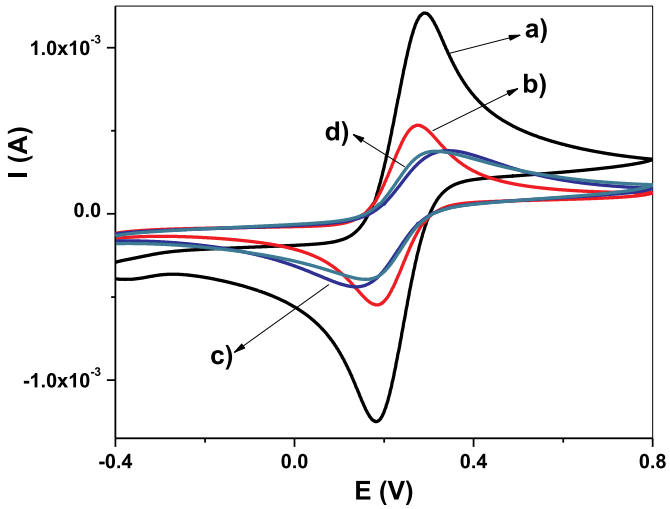

Fig. 3. Cyclic voltammograms recorded in 1×10^{-3} mol L^{-1} $[Fe(CN)_6]^{-4/-3}$ + 0.1 mol L^{-1} KCl aqueos solution at a) GCE, b) GCE/CRGO-βCD's, c) GCE/CRGO-βCD's/ADA-SPE and d) GCE/CRGO-βCD's/ADA-SPE/AuNPs.

(GCE/CRGO-βCD′s/ADA-SPE/AuNPs) produced an improvement in the electron transfer of the $[Fe(CN)_6]^{-4/-3}$ redox couple, which implies a decrease in the value of the R_{ET}. From the best fitting, a value of $R_{ET} = 627\ \Omega$ was obtained for GCE/CRGO-βCD′s/ADA-SPE/AuNPs.

Fig. 3 shows cyclic voltammperograms recorded for each one of the stages of modification of the electrode surface during the construction of the biosensor using 1×10^{-3} mol L^{-1} $[Fe(CN)_6]^{-4/-3}$ + 0.1 mol L^{-1} KCl aqueous solutions.

The anodic peak currents ($I_{p,a}$) and cathodic peak currents ($I_{p,c}$) of the $[Fe(CN)_6]^{-4/-3}$ redox couple decrease at the modified electrodes (GCE/CRGO-βCD′s (line b, Fig. 3)), GCE/CRGO-βCD′s/ADA-SPE (line c, Fig. 3) and GCE/CRGO-βCD′s/ADA-SPE/AuNPs (line d, Fig. 3) compared with the unmodified electrode (line a, Fig. 3).

For the GCE/CRGO-βCD′s a decrease for $I_{p,a}$ and $I_{p,c}$ are obtained respect to those of GCE (compare lines a with b in Fig. 3). This is because to the fact that the CRGO-βCD composite acts as an insulator, due in part to the oxygenated groups present in the GO that remain unreduced. In addition, the presence of βCD's can act as a separator between the sheets of CRGO hindering the discharge of the $[Fe(CN)_6]^{-4/-3}$ redox couple. However, there is a slight decrease in the difference between anodic and cathodic peak potentials (ΔE_p) at the modified electrode compare with the bare of GCE. On the other hand, when the ADA-SPE conjugate is added on the electrode surface (giving GCE/CRGO-βCD′s/ADA-SPE) a new decay of the $I_{p,a}$ and $I_{p,c}$ and an increase in ΔE_p is obtained. This can be explained considering that ADA-SPE acts as a dielectric layer, hindering the electron transfer of $[Fe(CN)_6]^{-4/-3}$ redox couple. Besides, the electro-deposition of the AuNPs at GCE/CRGO-βCD′s/ADA-SPE (GCE/CRGO-βCD′s/ADA-SPE/AuNPs) produced a slight improvement in the electron transfer of the redox couple (line d, Fig. 3).

3.3.2. Scanning electron microscopy with energy dispersive spectroscopy (SEM-EDS)

The surface morphology of the different stages of biosensor construction was investigated from SEM and EDS images. Fig. 4 displays typical SEM images for A) GCE/CRGO-βCD′s, B) GCE/CRGO-βCD′s/ADA-SPE, C) GCE/CRGO-βCD′s/ADA-SPE/AuNPs, and Fig. 4D shows the corresponding EDS image for GCE/CRGO-βCD′s/ADA-SPE/AuNPs. Fig. 4A shows the wrinkles and folds characteristic of CRGO. When conjugate ADA-SPE is added to the electrode modified with CRGO-βCD′s, significant changes in surface roughness occur (Fig. 4B). The surface morphology of electrode GCE/CRGO-βCD′s/ADA-SPE does not change significantly after electro-generation of AuNPs (Fig. 4C). This figure shows the appearance of small deposits on the surface of the electrode, of a size of 15 nm. In order to confirm the origin and distribution of these small deposits, Fig. 4D shows a micrograph obtained with elemental analysis by EDS. Thus, it is possible to observe that these deposits are due to electro-generated AuNPs and that they are homogeneously distributed over the surface of the modified electrode. In addition, Table 1 shows the percentage of each of the elements detected on the surfaces. Thus, only C and O are present at the GCE/CRGO-βCD′s surface. However, in addition to C and O, it was possible to detect the presence of Fe at the GCE/CRGO-βCD′s/ADA-SPE surface, which is related to the characteristic heme group of peroxidases. On the other hand, the presence of Au is detected at GCE/CRGO-βCD′s/ADA-SPE/AuNPs (Table 1).

Table 1
Percentage composition of the elements present in the different modified electrodes.

Element	GCE/CRGO-βCD′s	GCE/CRGO-βCD′s/ADA-SPE	GCE/CRGO-βCD′s/ADA-SPE/AuNPs
	% Atomic	% Atomic	% Atomic
C	92	80	78
O	7	19	21
Fe		0.01	0.01
Au			0.08

3.4. Determination of EUG

The potential applied to GCE/CRGO-βCD/ADA-SPE/AuNPs during the stabilization process and EUG aggregates is related to reduction of a quinone (derived from EUG) for giving the corresponding catechol. This

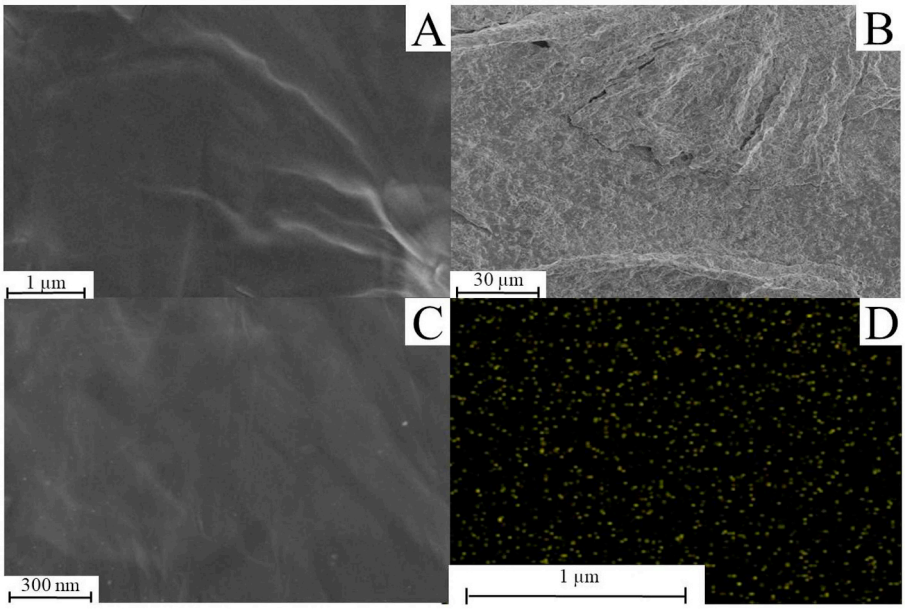

Fig. 4. SEM images of A) GCE/CRGO-βCD′s, B) GCE/CRGO-βCD′s/ADA-SPE and C) GCE/CRGO-βCD′s/ADA-SPE/AuNPs, and D) EDS micrograph of GCE/CRGO-βCD′s/ADA-SPE/AuNPs.

quinone is the product of the enzymatic reaction between SPE and EUG. Kaffash et al. [45] describe that the enzymatic oxidation of phenols through peroxidases gives an electroactive o-quinones. This reaction occurs in three steps giving as product the corresponding 4-allyl-o-quinone. Then, this 4-allyl-o-quinone produced can be reversibly reduced to 4-allyl-catechol at the electrode surface, as shown in Fig. S4 (Supplementary material). The electrochemical current, attributed to the reduction of 4-allyl-o-quinone is proportional to the concentration of 4-allyl-o-quinone and, it is directly related to the concentration of EUG in solution.

Figure S4A (Supplementary material) shows the cyclic voltammograms recorded at GCE/CRGO-βCD's/ADA-SPE/AuNPs in pH 7.0 PBS in the absence (line a) and in the presence (line b) of EUG. In the presence of EUG there is an anodic peak at about 0.4 V, which is attributed to the electrochemical oxidation of EUG. The small shoulder centered at approximately 0.2 V could be due to a small amount of the product of the EUG electrochemical oxidation adsorbed at the electrode surface. When the direction of the potential sweep is reversed, a cathodic peak is observed at about 0.1 V which is attributed to the reduction of the oxidation product of EUG. The peak centered at about – 0.5 V could be attributed to the reduction of oxygenated groups still present in the CRGO. Figure S4B (Supplementary material) shows a cyclic voltammogram recorded when H_2O_2 was added to the electrochemical cell in the presence of EUG. Due to the catalytic reaction of SPE on EUG, the 4-allyl-o-quinone generation occurs. At a potential of – 0.2 V, this quinone is reduced to the corresponding 4-allyl-cathecol. Thus, the cathecol is oxidized (peak I_a) during the anodic scan, and when the direction of the potential sweep is reversed, the corresponding quinone is reduced (peak I_c). Peaks are centered at 0.24 and 0.18 V, respectively. Thus, in the amperometric measurements at a potential of 0 V the changes in currents obtained are due to the transformation of the enzymatically generated 4-allyl-o-quinone to its corresponding 4-allyl-cathecol on the electrode surface.

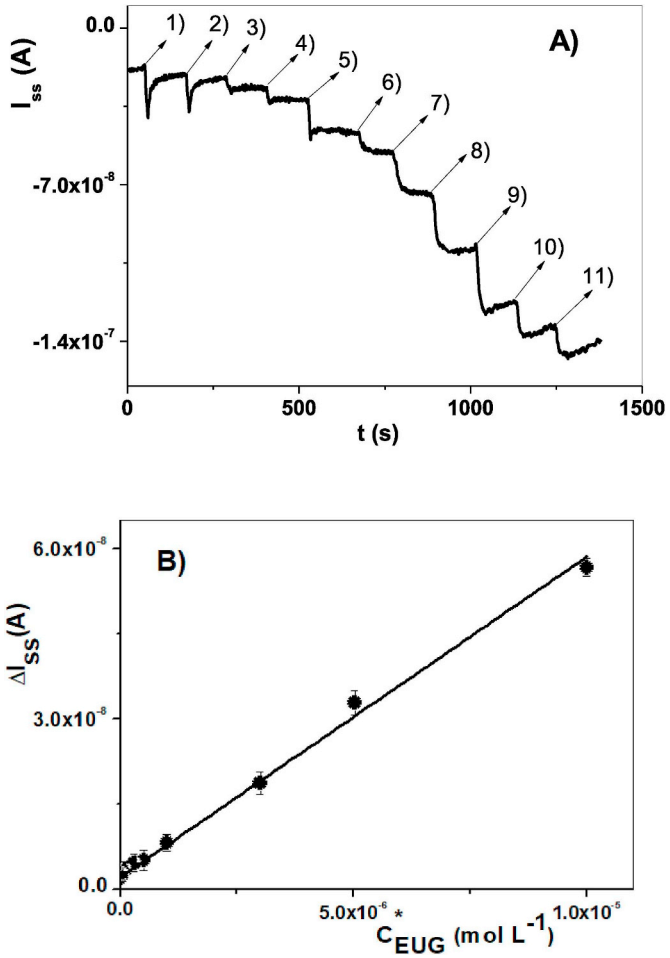

Fig. 5. A) I_{ss} vs. t for different aliquots of EUG. 1) 1×10^{-7}, 2) 3×10^{-7}, 3) 5×10^{-7}, 4) 1×10^{-6}, 5) 3×10^{-6}, 6) 5×10^{-6}, 7) 1×10^{-5}, 8) 3×10^{-5}, 9) 6×10^{-5}, 10) 8×10^{-5} and 11) 1×10^{-4} mol L^{-1}. B) ΔI_{ss} vs. c^*_{EUG} plot. The linear section of the calibration curve, which can be expressed by the linear least squares procedure as: $\Delta I_{ss} = (5.3 \pm 0.3) \times 10^{-3} \times c^*_{EUG}$ (mol L^{-1}) + $(2.0 \pm 0.1) \times 10^{-9}$ (A). Linear correlation coefficient, r = 0.9985.

Fig. 5A shows the steady-state reduction currents (I_{ss}) obtained after the addition of different EUG aliquots, in the presence of 1×10^{-4} mol L^{-1} H_2O_2. The steady state condition is reached at 30 s. The electro-deposition of AuNPs on the surface of the biosensor produced a slight increase in the redox couple reversibility as it can be inferred from cyclic voltammograms of Fig. 3, and a decrease in the signal stabilization time after the different aggregates of EUG compared to that the biosensor without AuNPs (results no shown). Fig. 5B shows the corresponding calibration curve (ΔI_{ss} vs c^*_{EUG}). Each point of the calibration curve is the average of five replicated measurements obtained using different GCE/CRGO-βCD's/ADA-SPE/AuNPs.

Biosensor sensitivity was $(5.3 \pm 0.3) \times 10^{-3}$ A mol^{-1} L. The linear concentration range was from 1.3×10^{-8} M to 1×10^{-5} mol L^{-1}. The limit of detection (LOD) measured with the GCE/CRGO-βCD's/ADA-SPE/AuNPs biosensor for a signal to noise ratio of 3:1 was 4×10^{-9} mol L^{-1}. The quantification limit (LOQ) calculated for a signal to noise ratio of 10:1 were 1.3×10^{-8} mol L^{-1}.

The GCE/CRGO-βCD's/ADA-SPE/AuNPs biosensor reproducibility was tested by measuring the sensibility of the corresponding calibration curves of five different bio-electrodes for the determination of EUG in pH 7.0 PBS containing 1×10^{-4} mol L^{-1} H_2O_2. Therefore, the intraday and inter-day were percentage variation coefficients (VC%) were 5% and 8%, respectively. Repeatability was determined by measuring the sensibility of five calibration curves obtained with the same GCE/CRGO-βCD's/ADA-SPE/AuNPs biosensor. A VC% of 3% was calculated. The biosensor was stable during twenty one days stored at 4 °C. A decrease of 30% in current responses was observed after the fourth week.

These values are similar but some parameters are better than those found in the literature for EUG using other electrochemical methods (Table 2). The lowest LOD for the determination of EUG has been achieved using GCE/CRGO-βCD's/ADA-SPE/AuNPs biosensor. Although the upper limit of the linear range is higher in some methods [12,20], in others they are of the same order of magnitude, but the lowest limit is achieved with our biosensor. On the other hand, the biosensor stability is similar to that reported in literature. In addition, it should be emphasized that the biosensor proposed in this paper is the first based on the use of an enzyme for the determination of EUG en dental samples.

The Michaelis-Menten apparent constant (K_M^{app}) was determined through both the Lineweaver-Burk (Eq. (1)) and Eadi-Hofstee (Eq. (2)) methods [27].

Table 2
Comparison of results obtained by the proposed method with other electrochemical methods found in the literature.

Electrode	Linear range (μmol L^{-1})	LOD (μmol L^{-1})	Stability (days)	Ref.
GCE/PDDA-G-MoS_2/Au	0.1–440	0.036	15	[12]
AuNPs/CPE	5–250	2	–	[20]
Cu@AuNPs/GCE	0.3–4.9	0.25	–	[21]
G/CPE	0.1–17	0.007	–	[22]
(G-CNTs-IL)/GCE/MIP	0.5–20	0.1	20	[23]
Graphene modified CPE	0.1–17	0.007	–	[46]
Pencil graphite electrode	0.3–50	0.085	–	[47]
GCE/CRGO-βCD's/ ADA-SPE/AuNPs	0.013–10	0.004	15	This work

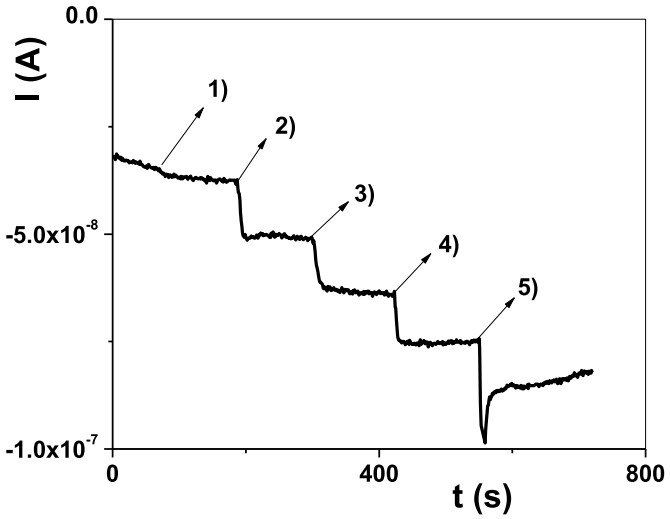

Fig. 6. Responses of the biosensor to the addition of a given aliquot of the local oral analgesic solution (1) and different aliquots (2–5) of the EUG commercial solution. $c^{*}_{EUG} = 3.5 \times 10^{-6}, 5 \times 10^{-6}, 7.5 \times 10^{-6}, 1 \times 10^{-5}$ mol L^{-1} from (2) to (5), respectively.

$$\frac{1}{I_{ss}} = \frac{1}{I_{max}} + \frac{K_M^{app}}{I_{max}} c^{*}_{EUG} \quad (1)$$

$$I_{ss} = -K_M^{app} \frac{I_{ss}}{c^{*}_{EUG}} + I_{max} \quad (2)$$

where I_{max} is the current obtained at the maximum reaction rate, under saturation conditions. From both methods a value of K_M^{app} of 3.1×10^{-6} mol L^{-1} was obtained. This value of K_M^{app} is in good agreement with others obtained by us for other analytes, demonstrating that EUG is a good co-substrate of peroxidase enzymes [48–50].

3.5. Determination of EUG in real samples

The GCE/CRGO-βCD's/ADA-SPE/NPsAu biosensor was used to determine EUG in two samples of dental use (a local oral analgesic treatment medicine and an intermediate restoration cement kit).

For the oral analgesic sample (Sample 1) it was only necessary to make a 1:100 dilution in 0.2 mol L^{-1} pH 7.0 PBS. The determination of EUG in these samples was carried out using the method of standard additions. After stabilizing the biosensor in the pH 7.0 PBS, an aliquot of the diluted solution was injected into the electrochemical cell at a final volume of 2 mL. Then, different aliquots of the EUG commercial solution were added every 2 min. Fig. 6 shows the amperograms obtained after these additions. Table 3 shows the concentrations of EUG of the prepared solutions from the oral analgesic sample (EUG concentration declared by the manufacturer is 0.3 mol L^{-1}) and those determined using the method of standard additions, with the corresponding recovery percentages (% R).

On other hand, the GCE/CRGO-βCD's/ADA-SPE/AuNPs biosensor was used to determine EUG in another dental sample (Sample 2). This sample is an intermediate restoration cement kit, which it is composed to a EUG solution (dissolved in acetic acid) and a powder containing ZnO and methyl polymethacrylate (EUG concentration declared by the manufacturer is 2.5×10^{-3} mol L^{-1}). The determination of EUG in this sample was also carried out using also the method of standard additions. In this kit, two different types of experiments were performed. On the one hand, EUG was determined in the liquid sample of the kit (Sample 2A) only by performing a dilution and subsequent addition to the cell (data not shown). On the other hand, the intermediate restoration cement was prepared as indicated by the manufacturer. Subsequently, the prepared paste was extracted with pH 7.0 PBS (in a 1:2 ratio of paste/PBS) and left to rest overnight. This was done because when the EUG joins the ZnO a chelation reaction occurs, forming zinc eugenolate (ZOE). When the ZOE is exposed to an aqueous medium such as saliva (pH 7.0 PBS in our experience), hydrolysis occurs, giving EUG and ZnOH [51]. Then, a sample aliquot (Sample 2B) was extracted from the supernatant of the previous preparation and a 1: 100 dilution was carried out. Table 3 shows the concentrations of the used solutions and those calculated using the standard additions method, with the corresponding recovery percentages.

The recovery percentages of EUG in the samples were between 94 and 108%. These results show that GCE/CRGO-βCD's/ADA-SPE/AuNPs can be applied to determine EUG efficiently in real samples, such as a local oral analgesic treatment medicine and an intermediate restoration cement kit.

4. Conclusions

A GCE/CRGO-βCD's/ADA-SPE/AuNPs biosensor was successfully developed for the determination of eugenol in dental samples. The GCE/CRGO-βCD's/ADA-SPE/AuNPs biosensor exhibited a very good performance for the quantification of eugenol. Thus, this biosensor shows a linear range between 1.3×10^{-8} and 1×10^{-5} mol L^{-1}, with a sensitivity of $(5.3 \pm 0.3) \times 10^{-4}$ A mol^{-1} L. The limits of detection and quantification were 4×10^{-9} mol L^{-1} and 1.3×10^{-8} mol L^{-1}, respectively. Biosensors have an intraday and inter days reproducibility

Table 3
Determination de EUG in dental samples.

c^{*}_{EUG} added (mol L^{-1})	Sample 1		Sample 2A		Sample 2B	
	c^{*}_{EUG} found[a] (mol L^{-1})	% R[b]	c^{*}_{EUG} found[a] (mol L^{-1})	% R[b]	c^{*}_{EUG} found[a] (mol L^{-1})	% R[b]
5×10^{-7}	$(4.7 \pm 0.1) \times 10^{-7}$	94			$(5.4 \pm 0.1) \times 10^{-7}$	108
1×10^{-6}	$(9.8 \pm 0.4) \times 10^{-7}$	98				
3×10^{-6}					$(2.9 \pm 0.3) \times 10^{-6}$	97
3.5×10^{-6}			$(3.4 \pm 0.4) \times 10^{-6}$	97		
5×10^{-6}	$(5.3 \pm 0.4) \times 10^{-7}$	107			$(4.9 \pm 0.4) \times 10^{-6}$	97
7×10^{-6}			$(7.0 \pm 0.3) \times 10^{-6}$	100		
1.3×10^{-5}			$(1.3 \pm 0.4) \times 10^{-5}$	100		

Sample 1: oral analgesic sample.
Sample 2A and 2B: intermediate restoration cement kit (see text).
[a] Mean value ± standard deviation.
[b] Recovery porcentaje.

of 5% and 8%, respectively. A repeatability of 3%, and a stability of 21 days (a decrease of 30% in current responses was observed after the fourth week.). Recovery studies were performed in order to validate the proposed method. Recovery percentages of the samples varied between 94 and 108%. The value of the apparent Michaellis-Menten constant, K_M^{app}, was $3.1 \times 10^{-6} \times 10^{-6}$ mol L^{-1} obtained by using both Lineweaver-Burk and Eadi-Hofstee methods.

Acknowledgements

Financial supports from Agencia Nacional de Promoción Científica y Tecnológica (FONCYT) (PICT 2266/2014), Consejo Nacional de Investigaciones Científicas y Técnicas (CONICET) (PIP 112-201101-00184), Ministerio de Ciencia y Tecnología de la Provincia de Córdoba (MINCyT) (PID 050/2010), and Secretaría de Ciencia y Técnica. (SECyT) (PPI 2016–2019, Res. 331/16 and Res. 068/19) from Universidad Nacional de Río Cuarto are gratefully acknowledged. J. C. Lopez thanks to CONICET for a doctoral fellowship.

Appendix A. Supplementary data

Supplementary data to this article can be found online at https://doi.org/10.1016/j.talanta.2019.120647.

References

[1] D.L. Madhavi, S.S. Deshpande, D.K. Salunkhe, Food Antioxidants. Technological, Toxicological, and Health Perspectives, Marcel Dekker, Inc., New York, USA, 1996.
[2] Y. Geng, J. Liu, R. Lv, J. Yuan, Y. Lin, X. Wang, An efficient method for extraction, separation and purification of eugenol from *Eugenia caryophyllata* by supercritical fluid extraction and high-speed counter-current chromatography, Separ. Purif. Technol. 57 (2007) 237–241, https://doi.org/10.1016/j.seppur.2007.04.015.
[3] R. Wang, R. Wang, B. Yang, Extraction of essential oils from five cinnamon leaves and identification of their volatile compound compositions, Innov. Food Sci. Emerg. Technol. 10 (2009) 289–292, https://doi.org/10.1016/j.ifset.2008.12.002.
[4] L. Alexandru, G. Cravotto, L. Giordana, A. Binello, F. Chemat, Ultrasound-assisted extraction of clove buds using batch- and flow-reactors: a comparative study on a pilot scale, Innov. Food Sci. Emerg. Technol. 20 (2013) 167–172, https://doi.org/10.1016/j.ifset.2013.07.011.
[5] S. Ghosh, D. Chatterjee, S. Das, P. Bhattacharjee, Supercritical carbon dioxide extraction of eugenol-rich fraction from *Ocimum sanctum Linn* and a comparative evaluation with other extraction techniques: process optimization and phytochemical characterization, Ind. Crops Prod. 47 (2013) 78–85, https://doi.org/10.1016/j.indcrop.2013.02.030.
[6] S.O. Oyedemi, A.I. Okoh, L.V. Mabinya, G. Pirochenva, A.J. Afolayan, The proposed mechanism of bactericidal action of eugenol, α-terpineol and γ-terpinene against *Listeria monocytogenes, Streptococcus pyogenes, Proteus vulgaris* and *Escherichia coli*, Afr. J. Biotechnol. 8 (2009) 1280–1286.
[7] N. Didry, L. Dubreuil, M. Pinkas, Activity of thymol, carvacrol, cinnamaldehyde and eugenol on oral bacteria, Pharm. Acta Helv. 69 (1994) 25–28, https://doi.org/10.1016/0031-6865(94)90027-2.
[8] S.K. Jaganathan, E. Supriyanto, Antiproliferative and molecular mechanism of eugenol-induced apoptosis in cancer cells, Molecules 17 (2012) 6290–6304, https://doi.org/10.3390/molecules17066290.
[9] S. Akbari, M.J. Khoshnod, H. Rajaian, M. Afsharnasab, The use of eugenol as an anesthetic in transportation of with Indian shrimp (*Fenneropenaeus indicus*) post larvae, Turk. J. Fish. Aquat. Sci. 10 (2010) 423–429, https://doi.org/10.4194/trjfas.2010.0317.
[10] G.P. Kamatou, I. Vermaak, A.M. Viljoen, Eugenol-from the remote Maluku Islands to the international market place: a review of remarkable and versatile molecule, Molecules 17 (2012) 6953–6981, https://doi.org/10.3390/molecules17066953.
[11] World Health Organization (WHO), WHO Food Additives Series: 56, Safety Evaluation of Certain Food Additives, Geneva (2006).
[12] Q. Feng, K. Duan, X. Ye, D. Lu, Y. Du, C. Wang, A novel way for detection of eugenol via poly (diallyldimethylammonium chloride) functionalized graphene-MoS_2 nanoflower fabricated electrochemical sensor, Sens. Actuators B Chem. 192 (2014) 1–8, https://doi.org/10.1016/j.snb.2013.10.087.
[13] P.C. Frohlich, K.A. Santos, F. Palúa, L. Cardozo-Filho, C. da Silva, E. Antônio da Silva, Evaluation of the effects of temperature and pressure on the extraction of eugenol from clove (*Syzygium aromaticum*) leaves using supercritical CO_2, J. Supercrit. Fluids 143 (2019) 313–320, https://doi.org/10.1016/j.supflu.2018.09.009.
[14] C.D. Hatrick, W.S. Eakle, W.F. Bird, Dental Materials: Clinical Applications for Dental Assistants and Dental Hygienists, second ed., Saunders Elseviers, Philadelphia, USA, 2010.
[15] L.-H. Wang, W.-C. Sung, Rapid evaluation and quantitative analysis of eugenol derivatives in essential oils and cosmetic formulations on human skin using attenuated total reflectance–infrared spectroscopy, Spectroscopy 26 (2011) 43–52, https://doi.org/10.3233/SPE-2011-0526.
[16] J.G. Lisko, S.B. Stanfill, C.H. Watson, Quantitation of ten flavor compounds in unburned tobacco products, Anal. Methods 6 (2014) 4698–4704, https://doi.org/10.1039/C4AY00271G.
[17] B. Yu, S. Lai, Q. Tan, Simultaneous determination of cinnamaldehyde, eugenol and paeonol in traditional Chinese medicinal preparations by cappillary GC-FID, Chem. Pharm. Bull. 54 (2006) 114–116, https://doi.org/10.1248/cpb.54.114.
[18] K. Schulz, K. Schlenz, S. Malt, R. Metasch, W. Romhild, J. Drebler, D.W. Lachenmeir, Headspace solid-phase microextraction-gas chromatography-mass spectrometry for the quantitative determination of the characteristic flavouring agent eugenol in serum samples after enzymatic cleavage to validate post-offence alcohol drinking claims, J. Chromatogr. A 1211 (2008) 113–119, https://doi.org/10.1016/j.chroma.2008.09.068.
[19] V.D. Thyagaraj, R. Koshy, M. Kachroo, A.S. Mayachari, L.P. Sawant, M. Balasubramanium, A validated RP-HPLC-UV/DAD method for simultaneous quantitative determination of rosmarinic acid and eugenol in *Ocimum sanctum L.* Pharm. Methods 4 (1) (2013) 1–5, https://doi.org/10.1016/j.phme.2013.08.003.
[20] d. Afzali, S. Zarei, F. Fathirad, A. Mostafavi, Gold nanoparticles modified carbon paste electrode for differential pulse voltammetric determination of eugenol, Mater. Sci. Eng. C 43 (2014) 97–101, https://doi.org/10.1016/j.msec.2014.06.035.
[21] X. Lin, Y. Ni, S. Kokot, Electrochemical mechanism of eugenol at a doped gold nanoparticles modified glassy carbon electrode and its analytical application in food samples, Electrochim. Acta 133 (2014) 484–491, https://doi.org/10.1016/j.electacta.2014.04.065.
[22] G. Yildiz, Z. Aydogmus, M.E. Cinar, F. Senkal, T. Ozturk, Electrochemical oxidation mechanism of eugenol on graphene modified carbon paste electrode and its analytical application to pharmaceutical analysis, Talanta 173 (2017) 1–8, https://doi.org/10.1016/j.talanta.2017.05.056.
[23] L. Yang, F. Zhao, B. Zeng, Electrochemical determination of eugenol using a three-dimensional molecularly imprinted poly (p-aminothiophenol-co-p-aminobenzoic acids) film modified electrode, Electrochim. Acta 210 (2016) 293–300, https://doi.org/10.1016/j.electacta.2016.05.167.
[24] C.I.L. Justino, A.C. Duarte, T.A.P. Rocha-Santos, Critical overview on the application of sensors and biosensors for clinical analysis, Trends Anal. Chem. 85 (2016) 36–60, https://doi.org/10.1016/j.trac.2016.04.004.
[25] J.P. Mc Eldoon, J.S. Dordick, Unusual thermal stability of soybean peroxidase, Biotechnol. Prog. 12 (1996) 555–558, https://doi.org/10.1021/bp960010x.
[26] J.K.A. Kamal, D.V. Behere, Activity, stability and conformational flexibility of seed coat soybean peroxidase, J. Inorg. Biochem. 94 (2003) 236–242, https://doi.org/10.1016/S0162-0134(03)00004-7.
[27] C.H. Díaz Nieto, A.M. Granero, J.C. Lopez, G.D. Pierini, G.J. Levin, H. Fernández, M.A. Zon, Development of a third generation biosensor to determine hydrogen peroxide based on a composite of soybean peroxidase/chemically reduced graphene oxide deposited on glassy carbon electrodes, Sens. Actuators B Chem. 263 (2018) 377–386, https://doi.org/10.1016/j.snb.2018.02.094.
[28] C.H. Díaz Nieto, A.M. Granero, D. Garcia, A. Nesci, G. Barros, M.A. Zon, H. Fernández, Development of a third-generation biosensor to determine sterigmatocystin mycotoxin: an early warning system to detect aflatoxin B1, Talanta 194 (2019) 253–258, https://doi.org/10.1016/j.talanta.2018.10.032.
[29] M. Lv, X. Wang, J. Li, X. Yang, C. Zhang, J. Yang, H. Hu, Cyclodextrin-reduced graphene oxide hybrid nanosheets for the simultaneous determination of lead (II) and cadmium (II) using square wave anodic stripping voltammetry, Electrochim. Acta 108 (2013) 412–420, https://doi.org/10.1016/j.electacta.2013.06.099.
[30] Y. Guo, S. Guo, J. Ren, Y. Zhai, S. Dong, E. Wang, Cyclodextrin functionalized graphene nanosheets with high supramolecular recognition capability: synthesis and host-guest inclusion for enhanced electrochemical performance, ACS Nano 4 (2010) 4001–4010, https://doi.org/10.1021/nn100939n.
[31] D. Lu, S. Lin, L. Wang, X. Shi, C. Wang, Y. Zhang, Synthesis of cyclodextrin-reduced graphene oxide hybrid nanosheets for sensitivity enhanced electrochemical determination of diethylstilbestrol, Electrochim. Acta 85 (2012) 131–138, https://doi.org/10.1016/j.electacta.2012.07.071.
[32] A. Fragoso, J. Caballero, E. Almirall, R. Villalonga, R. Cao, Immobilization of adamantane-modified cytochorome c at electrode surfaces through supramolecular interactions, Langmuir 18 (2002) 5051–5054, https://doi.org/10.1021/la0256679.
[33] R. Villalonga, C. Camacho, R. Cao, J. Hernández, J.C. Matías, Amperometric biosensor for xanthine with supramolecular architecture, Chem. Commun. (2007) 942–944, https://doi.org/10.1039/B614997A.
[34] L.-M. Lu, X.-L. Qiu, X.-B. Zhang, G.-L. Shen, W. Tan, R.-Q. Yu, Supramolecular assembly of enzyme on functionalized graphene for electrochemical biosensing, Biosens. Bioelectron. 45 (2013) 102–107, https://doi.org/10.1016/j.bios.2013.01.065.
[35] X. Wang, X. Zhang, Electrochemical co-reduction synthesis of graphene/nano-gold composites and its application to electrochemical glucose biosensor, Electrochim. Acta 112 (2013) 774–782, https://doi.org/10.1016/j.electacta.2013.09.036.
[36] A. Benvidi, A. Dehghani-Firouzabadi, M. Mazloum-Ardakani, B. Mirjalili, R. Zare, Electrochemical deposition of gold nanoparticles on reduced graphene oxide modified glassy carbon electrode for simultaneous determination of levodopa, uric acid and folic acid, J. Electroanal. Chem. 736 (2015) 22–29, https://doi.org/10.1016/j.jelechem.2014.10.020.
[37] B. Wu, N. Zhao, S. Hou, C. Zhang, Electrochemical synthesis of polypyrrole, reduced graphene oxide, and gold nanoparticles composite and its application to hydrogen peroxide biosensor, Nanomaterials 6 (2016) 220–231, https://doi.org/10.3390/nano6110220.
[38] A.G. Hildebrandt, I. Roots, Reduced nicotinamide adenine dinucleotide phosphate (NADPH) dependent formation and breakdown of hydrogen peroxide during mixed function oxidation reactions in liver microsomes, Arch. Biochem. Biophys. 171

(1975) 385–397, https://doi.org/10.1016/0003-9861(75)90047-8.
[39] J.K.A. Kamal, D.V. Behere, Activity, stability and conformational flexibility of seed coat soybean peroxidase, J. Inorg. Biochem. 94 (2003) 236–242, https://doi.org/10.1016/S0162-0134(03)00004-7.
[40] D.C. Marcano, D.V. Kosynkin, J.M. Berlin, A. Sinitskii, Z. Sun, A. Slesarev, L.B. Alemany, W. Lu, J.M. Tour, Improved synthesis of graphene oxide, ACS Nano 4 (2010) 4806–4814, https://doi.org/10.1021/nn1006368.
[41] Y. Guo, S. Guo, J. Li, E. Wang, S. Dong, β-Cyclodextrin-graphene hybrid nanosheets as enhanced sensing platform for ultrasensitive determination of carbendazim, Talanta 84 (2011) 60–64, https://doi.org/10.1016/j.talanta.2010.12.007.
[42] D. Montgomery, G. Runger, Probabilidad Y Estadística, second ed., Mc Graw Hill. Interamericana Editores, México, 2000.
[43] J.C. Lopez, M.A. Zon, H. Fernández, A.M. Granero, S.N. Robledo, Determination of kinetic parameters of the enzymatic reaction between soybean peroxidase and natural antioxidants using chemometric tools, Food Chem. 275 (2019) 161–168, https://doi.org/10.1016/j.foodchem.2018.08.145.
[44] E. Casero, A.M. Parra-Alfambra, M.D. Petit-Domínguez, F. Pariente, E. Lorenzo, C. Alonso, Differentiation between graphene oxide and reduced graphene by electrochemical impedance spectroscopy (EIS), Electrochem. Commun. 20 (2012) 63–66, https://doi.org/10.1016/j.elecom.2012.04.002.
[45] A. Kaffash, K. Rostami, H.R. Zare, Modeling of an electrochemical nanobiosensor in COMSOL multiphysics to determine phenol in the presence of horseradish peroxidase, Enzym. Microb. Technol. 121 (2019) 23–28, https://doi.org/10.1016/j.enzmictec.2018.11.001.
[46] Q. Feng, K. Duan, Xiaoliang Ye, D. Lu, Y. Du, C. Wang, Electrochemical oxidation mechanism of eugenol on graphene modified carbon paste electrode and its analytical application to pharmaceutical analysis, Sens. Actuators B Chem. 192 (2014) 1–8, https://doi.org/10.1016/j.snb.2013.10.087.
[47] Ö. Sağlam, D.G. Dilgin, B. Ertek, Y. Dilgin, Differential pulse voltammetric determination of eugenol at a pencilgraphite electrode, Mater. Sci. Eng. C 60 (2016) 156–162, https://doi.org/10.1016/j.msec.2015.11.031.
[48] A.M. Granero, H. Fernández, E. Agostini, M.A. Zon, An amperometric biosensor for trans-resveratrol determination in aqueous solutions by means of carbon paste electrodes modified withperoxidase basic isoenzymes from Brassica Napus, Electroanalysis 20 (2008) 858–864, https://doi.org/10.1002/elan.200704109.
[49] V.G.L. Zachetti, A.M. Granero, S.N. Robledo, M.A. Zon, Héctor Fernández, Development of an amperometric biosensor based on peroxidases to quantify citrinin in rice samples, Bioelectrochemistry 91 (2013) 37–43, https://doi.org/10.1016/j.bioelechem.2012.12.004.
[50] C.H. Díaz Nieto, A.M. Granero, D. Garcia, A. Nesci, G. Barros, M.A. Zon, H. Fernández, Development of a third-generation biosensor to determine sterigmatocystin mycotoxin: an early warning system to detect aflatoxin B1, Talanta 194 (2019) 253–258, https://doi.org/10.1016/j.talanta.2018.10.032.
[51] K. Markowitz, M. Moynihan, M. Liu, S. Kim, Biologic properties of eugenol and zinc oxide-eugenol, Oral surg, Oral Med. Oral Pathol. 73 (1992) 729–737, https://doi.org/10.1016/0030-4220(92)90020-q.